

## Constructing Integrable High-pressure Full-current Free-boundary Stellarator Magnetohydrodynamic Equilibrium Solutions.

S.R.Hudson 1), D.A.Monticello 1), A.H.Reiman 1), D.J.Strickler 2), S.P.Hirshman 2),  
L-P. Ku 1), E.Lazarus 2), A.Brooks 1), M.C.Zarnstorff 1), A.H.Boozer 3), G-Y. Fu 1) & G.H.Neilson 1).

1) Princeton Plasma Physics Laboratory, P.O. Box 451, Princeton NJ 08543, USA.

2) Oak Ridge National Laboratory, P.O. Box 2009, Oak Ridge TN 37831, USA.

3) Columbia University, New York, New York 10027, USA.

email contact of main author: shudson@pppl.gov

**Abstract.** For the (non-axisymmetric) stellarator class of plasma confinement devices to be feasible candidates for fusion power stations it is essential that, to a good approximation, the magnetic field lines lie on nested flux surfaces; however, the inherent lack of a continuous symmetry implies that magnetic islands responsible for breaking the smooth topology of the flux surfaces are guaranteed to exist. Thus, the suppression of magnetic islands is a critical issue for stellarator design, particularly for small aspect ratio devices. Pfirsch-Schlüter currents, diamagnetic currents and resonant coil fields contribute to the formation of magnetic islands, and the challenge is to design the plasma and coils such that these effects cancel.

Magnetic islands in free-boundary high-pressure full-current stellarator magnetohydrodynamic equilibria are suppressed using a procedure based on the Princeton Iterative Equilibrium Solver [Comp. Phys. Comm., 43:157, 1986] which iterates the equilibrium equations to obtain the plasma equilibrium. At each iteration, changes to a Fourier representation of the coil geometry are made to cancel resonant fields produced by the plasma. The changes are constrained to preserve certain measures of engineering acceptability and to preserve the stability of ideal kink modes. As the iterations continue, the coil geometry and the plasma simultaneously converge to an equilibrium in which the island content is negligible, the plasma is stable to ideal kink modes, and the coils satisfy engineering constraints. The method is applied to a candidate plasma and coil design for the National Compact Stellarator eXperiment [Phys. Plas. 8(5):2083, 2001].

### 1. Introduction

An attractive stellarator requires a set of non-axisymmetric coils that confines a high-pressure plasma so that the self-consistent plasma equilibrium currents and the coil currents combine to produce an integrable magnetic field. A perfectly integrable field is too stringent a requirement for practical purposes — if the perturbations are small, the theory of Kolmogorov, Arnol'd and Moser (KAM) [1] implies that flux surfaces will exist almost everywhere; and sufficiently small magnetic islands will have little, if any, effect on particle transport. In this context, ‘good-flux-surfaces’ indicates that the islands occupy less than a tolerable percentage of the plasma volume. Nevertheless, to construct magnetohydrodynamic (MHD) equilibria with high-pressure in which the island content is negligible is a challenging task.

Traditional stellarator design seeks to optimize plasma performance (particle orbits, MHD stability, etc.) subject to engineering constraints. These optimizations rely on plasma equilibrium codes, and the fastest stellarator equilibrium codes presuppose perfect flux surfaces — the existence or size of magnetic islands cannot be addressed. The flux surface quality is investigated using equilibrium codes which allow a general representation of the field including islands after the plasma and coils are designed. With such an approach, there is no guarantee that the configuration will have acceptable flux surface quality.

The difficulty of constructing plasma equilibria with integrable fields lies in part that the plasma itself is not controlled directly, but indirectly through coil design. Pfirsch-Schlüter currents, diamagnetic currents and resonant coil fields contribute to the formation of magnetic islands. The challenge is to design the plasma and coils such that these effects cancel. A recent article [2] presented a method by which high-pressure full-current *fixed*-boundary solutions may be constructed with good flux-surfaces. Small adjustments to the boundary were related to the resonant fields at rational rotational-transform surfaces and, by suitable boundary adjustment, magnetic islands were suppressed.

Stellarator coils may be designed to balance the coil field and the plasma field on a given boundary; but, practical considerations, such as cost, engineering constraints and diagnostic access, limit reconstruction accuracy [3]. To balance the coil field and the plasma field perfectly at every point on a given boundary requires a continuous current distribution on some prescribed surface, and if discretized will lead to

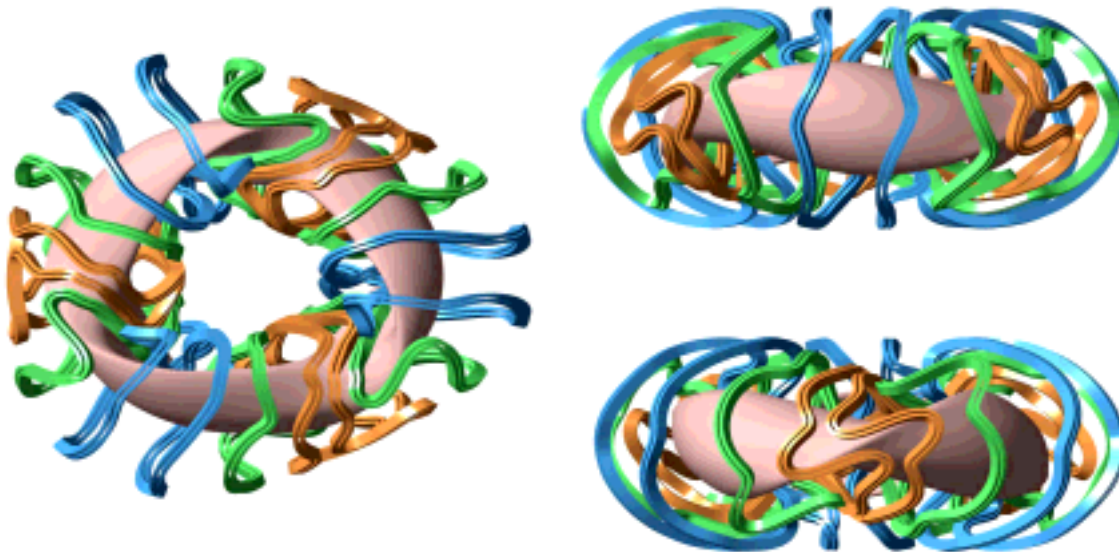


FIG. 1: The modular coils of NCSX.

singular coil currents [4]. The fixed boundary healing work [2] showed that for the suppression of islands, only a certain spectrum of modes of the normal field on a given boundary is related to island formation. Ultimately it is the resonant magnetic fields at the rational surfaces that cause islands. In the small island approximation, the width of an island depends on the magnitude of the resonant field,  $B_{nm}$ , and the shear,  $\epsilon'$ ,

$$\Delta = (|B_{nm}|/|\epsilon' m|)^{1/2}. \quad (1)$$

The phase of the island depends on the sign of both  $B_{nm}$  and  $\epsilon'$ . The fixed-boundary healing method, and the method to be described in this article, express the resonant fields as functions of a set of independent variables (boundary harmonics or coil geometry parameters). Standard numerical techniques may then be used to set  $B_{nm} = 0$ : thus eliminating islands.

This article describes a method for constructing high-pressure full-current free-boundary MHD equilibria with confining coils designed to suppress selected resonances. The method is based on the free-boundary Princeton Iterative Equilibrium Solver (PIES) code [5] which iterates the MHD equilibrium equations to solve for plasma equilibria in stellarator geometry. PIES does not constrain the magnetic field topology to preserve nested magnetic flux surfaces and, for an arbitrary coil set, will converge to an equilibrium with islands. Island suppression is achieved by modifying the coil geometry at each iteration so that selected resonant components of the coil magnetic field cancel the resonant components of the plasma magnetic field. It is of course necessary to ensure that the optimized plasma and engineering figures of merit are not compromised in this procedure. This is achieved by constraining the coil variations to lie in the nullspace of these figures of merit. As the iterations proceed, the coil geometry and the plasma simultaneously converge to an island-free coil-plasma equilibrium with the desirable plasma and coil properties preserved.

The method is applied to a stellarator design considered for the National Compact Stellarator eXperiment (NCSX) [6]. Features of the design make special demands on the coil design to avoid magnetic islands. NCSX is compact, thus the lack of symmetry is pronounced, and has a large shear and transform per period, which produce multiple low order resonances. A significant percentage of the rotational transform is provided by the plasma current and thus the vacuum rotational transform profile is quite different to the designed operating reference configuration. Consequently, the removal of islands in the vacuum state does not demonstrate the removal of islands in the full plasma current case. Also, NCSX will operate at high plasma pressure. The effect of pressure will modify the shape of the equilibrium flux surfaces, and thus modify the magnetic field spectrum produced by the coils at rational surfaces. In addition, magnetic islands themselves are directly affected by pressure [7], and equilibrium calculations using the HINT code [8] have shown that this can lead to an effect called ‘self-healing’ [9]. The finite- $\beta$  full-current reference configuration itself needs to be directly considered.

## 2. Method

The total magnetic field,  $\mathbf{B}$ , is the sum of the magnetic field produced by the plasma,  $\mathbf{B}_P$ , and the magnetic field produced by the confining coils,  $\mathbf{B}_C$ , which is a function of a set of Fourier harmonics,  $\boldsymbol{\xi}$ , that describe the coil geometry, at the  $n$ th PIES iteration

$$\mathbf{B}^n = \mathbf{B}_P^n + \mathbf{B}_C(\boldsymbol{\xi}^n). \quad (2)$$

The initial plasma state is provided by the combined NESTOR and VMEC codes [10, 11], to give the free-boundary VMEC code, which makes the artificial simplifying assumption that the plasma is consistent with nested flux-surfaces, and the initial coil geometry is provided by the COILOPT code [12]. The method presented in this article removes the constraint of nested flux-surfaces and allows the initialization to relax into an equilibrium, potentially with islands, while making adjustments to the coil set to remove selected islands as they develop. The PIES iterations solve for the plasma current  $\mathbf{J}$  given  $\mathbf{B}$  and the pressure profile,  $p$ ; and then the plasma magnetic field is solved given  $\mathbf{J}$

$$\nabla p = \mathbf{J}^{n+1} \times \mathbf{B}^n, \quad (3)$$

$$\mathbf{J}^{n+1} = \nabla \times \mathbf{B}_P^{n+1}. \quad (4)$$

The standard PIES algorithm makes no changes to the coil geometry and iterates through Eqns (3) and (4) to calculate the equilibrium for the given coils and pressure profile. The additional steps for coil-healing are as follows. The total magnetic field  $\mathbf{B}$  at this stage is

$$\mathbf{B}^{n+\frac{1}{2}} = \mathbf{B}_P^{n+1} + \mathbf{B}_C(\boldsymbol{\xi}^n). \quad (5)$$

The superscript  $n + \frac{1}{2}$  indicates that the intermediate total field  $\mathbf{B}$  has not yet advanced to the next iteration. At this stage, the plasma field has been updated, but the coil field has not. To avoid clumsy notation, the intermediate total field will be represented simply as  $\mathbf{B}$ .

We may consider  $\mathbf{B}$  to be a nearly integrable field, and that magnetic islands are caused by fields normal to, and resonant with, rational rotational-transform,  $\iota$ , flux-surfaces of a nearby integrable field. For each resonance selected for suppression, a quadratic-flux-minimizing surface [13] is constructed. A quadratic-flux-minimizing surface is a surface that extremizes the quadratic-flux functional

$$\varphi_2 = \frac{1}{2} \int \int \left[ \frac{\partial S}{\partial \theta} \right]^2 d\theta d\zeta, \quad (6)$$

where  $S$  is the magnetic field line action  $S = \oint \mathbf{A} \cdot d\mathbf{l}$ ,  $\mathbf{A}$  is the magnetic vector potential and  $\theta, \zeta$  are poloidal and toroidal coordinates. Each such surface may be considered as a rational flux-surface of an underlying integrable field [14], with each surface passing through its associated island chain. The construction of the quadratic-flux-minimizing surfaces provides an optimal magnetic coordinate system exactly and only where required — at the rational rotational-transform surfaces where islands develop. The amplitude of each resonant field harmonic is calculated by Fourier decomposing the field normal to the surface in an angle coordinate which corresponds to a straight field line coordinate of the integrable field on that surface. The selected set of resonant harmonic amplitudes thus calculated is denoted  $\{B_i : i = 1, N\}$ , where  $B_i = B_{n_i, m_i}$  is the  $(n_i, m_i)$  Fourier harmonic of  $(\mathbf{B} \cdot \nabla \psi / \mathbf{B} \cdot \nabla \zeta)$  calculated on the rational surface labeled by  $\psi$ .

The COILOPT [12] code provides a convenient Fourier representation of the coil geometry and an appropriate set of coil harmonics  $\{\xi_j : j = 1, M\}$  is systematically varied to set  $B_i = 0$  using a Newton method. The coupling matrix,  $\nabla B_{Cij}$ , is defined as the partial derivatives of the selected resonant harmonics of the coil magnetic field normal to the quadratic-flux-minimizing surface (held constant during each PIES/healing iteration) with respect to the chosen coil harmonics and is calculated using finite-differences. In the linear approximation, a multi-dimensional Newton method determines the coil changes  $\delta \xi_j^n$  that cancels the resonant fields

$$B_i + \sum_j \nabla B_{Cij} \cdot \delta \xi_j^n = 0. \quad (7)$$

This equation is solved for the  $\delta \xi_j^n$  in a few iterations by inverting the  $N \times M$  matrix  $\nabla B_{Cij}$  using singular value decomposition (SVD) [15] and the new coil set is obtained

$$\xi_j^{n+1} = \xi_j^n + \delta \xi_j^n, \quad (8)$$

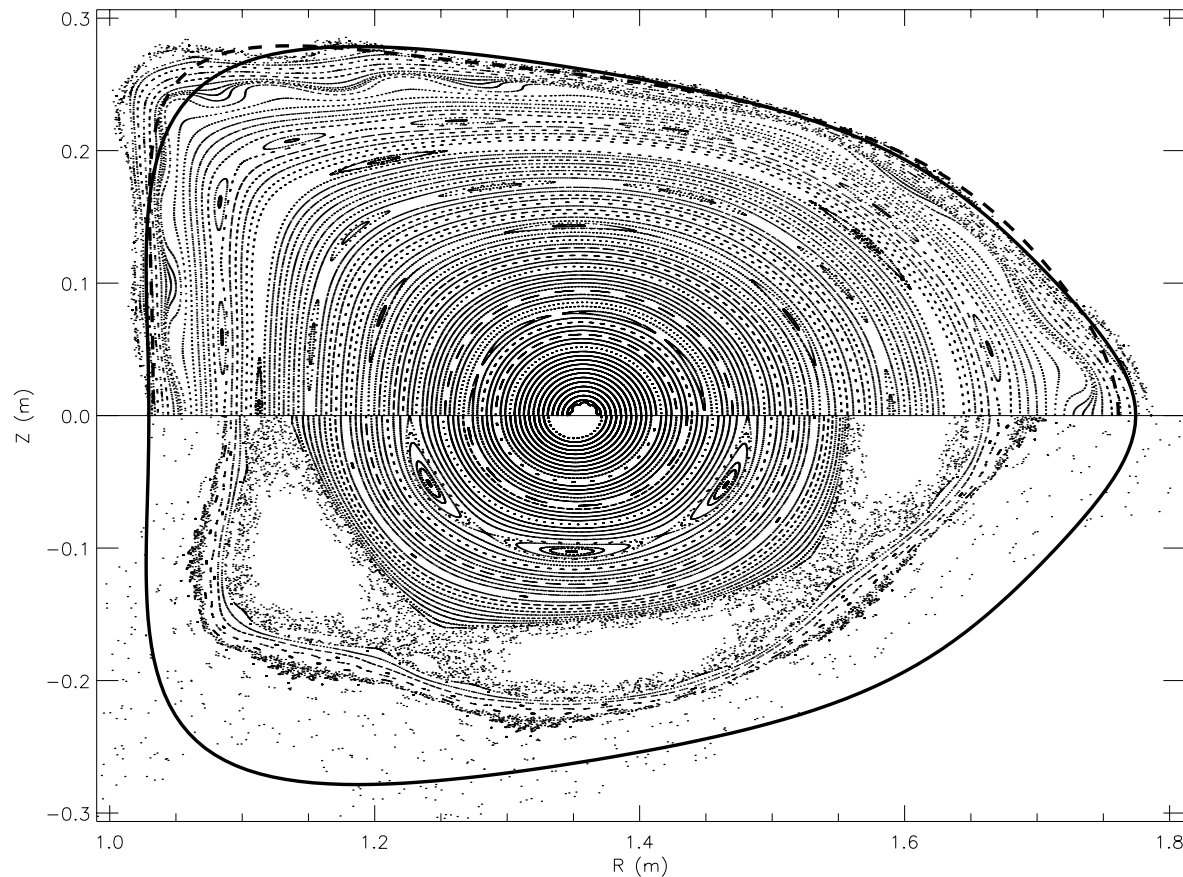


FIG. 2: Poincaré plot of converged healed coil-plasma configuration (upper) and of the original configuration (lower). The VMEC initialization boundary (solid line) and the boundary of the VMEC configuration consistent with the healed coils (dashed line – upper) are also shown.

such that the resonant component of the combined plasma-coil field is eliminated. By adjusting the coil geometry at every iteration, the inherent non-linearity of the plasma response is effectively controlled. As the iterations continue, the coil geometry and the plasma simultaneously converge to an equilibrium with good flux-surfaces.

The healing algorithm just described is augmented to include engineering constraints. The coils are represented by filaments (with zero cross-sectional area). It is required that the coil filaments are well separated to allow for finite thickness coils that will eventually be built. Also, there is a limit to how tightly the coils can bend. The initial coil set, described by  $\xi^0$ , is satisfactory from an engineering perspective. To include the engineering constraints, the vector  $B_i$  of resonant fields to be eliminated is augmented by including the (appropriately weighted) differences in coil-coil separation and minimum bend-radius (calculated by COILOPT) of the  $n$ th coil set, described by  $\xi^n$ , from the initial coil set. To the accuracy of the finite difference calculation of the coupling matrix, and to the validity of the linear approximation, this constrains the island eliminating coil variations to lie in the nullspace of these measures of engineering acceptability. Also, the kink stability of the free-boundary VMEC equilibrium for each trial coil set is computed using TERPSICHORE [16], and in a similar manner changes to the coil geometry are constrained to preserve kink stability. Finally, some numerical checks are performed to ensure that the suggested coil correction does in fact reduce the magnitude of the function vector  $|B_i|$ , and if not, the coil correction is rejected.

### 3. Application to NCSX

The method is routinely applied to NCSX [6] candidate coil and plasma designs. The plasma design adopted by NCSX has 3 field periods, is quasi-axisymmetric to give good transport and is stable to kink modes at  $\beta=4.1\%$ , but is marginally unstable to infinite  $n$  ballooning modes. The rotational-transform profile has  $\iota \approx 0.4$  on axis,  $\iota \approx 0.66$  near the edge and  $\iota \approx 0.65$  at the edge: including the low order resonances  $\iota = 3/7, 3/6$  and  $3/5$ . The coil design has 6 stellarator symmetric modular coils per period, shown in Fig.(1), and additional vertical field coils and trim coils.

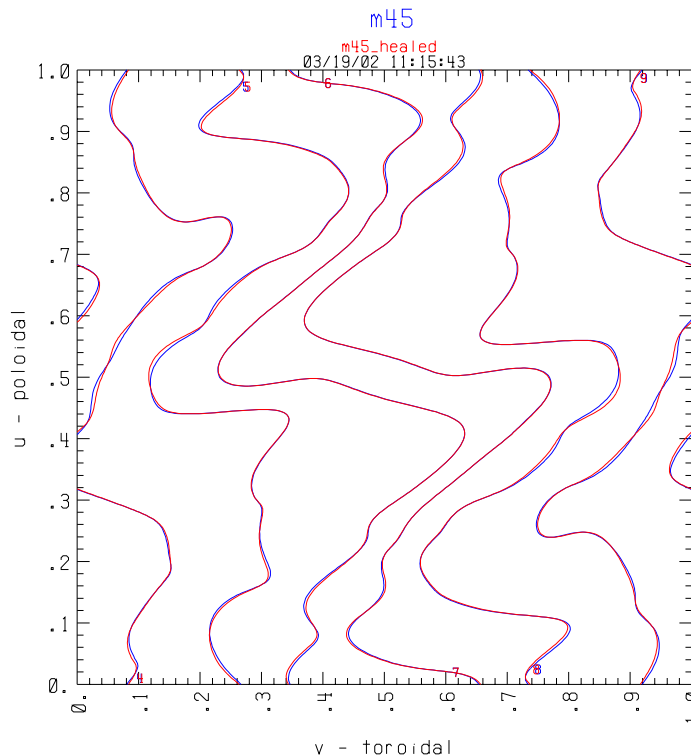


FIG. 3: Coil comparison showing the original coils and the healed coils on the toroidal winding-surface.

Considering a candidate coil set (named m45) and selecting the  $(n,m)=(3,6),(3,5)$  islands, together with the minimum bend-radius, coil-coil separation and kink stability (9 constraints), and allowing some  $m=3,4,5,6,7$  and 8 coil harmonics to vary (36 independent variables), a kink-stable healed-plasma equilibrium, with coils preserving the engineering measures, is obtained. Several hundred PIES/healing iterations are required to achieve convergence in the coil geometry. To confirm convergence in the plasma equilibrium, several hundred additional PIES iterations are performed with the coil geometry unchanged. A Poincaré plot of the final field is shown on an up-down symmetric toroidal cross section in Fig.(2).

Small high-order islands,  $(n,m) = (3,7), (6,12), (6,11), (6,10)$  and  $(9,14)$ , that have not been selected for reduction remain but these are considered tolerable. There is some resonant  $(n,m) = (12,18)$  deformation where  $\epsilon' = 0$  near the edge, which indicates that additional *near*-resonant fields may need to be eliminated. The plasma retains quasi-axisymmetry and is stable to finite- $n$  ballooning modes with  $n < 45$ . A Poincaré plot of the original configuration is shown after 180 standard PIES iterations and this case deteriorates into large regions of chaos as the iterations continue.

The boundary of the VMEC equilibrium consistent with the original coils is shown as the solid line. This equilibrium was used to initialize the PIES/healing run. The boundary of the VMEC equilibrium consistent with the healed coils is shown as the dashed line in the upper half of the plot. If the PIES equilibrium was perfectly healed, then it and the VMEC equilibrium should agree. The agreement between the PIES and VMEC boundaries is good, but not perfect. The difference may result from the existence of small residual islands in the PIES equilibrium. To investigate this further, it may be necessary to extend the coil healing to suppress the higher order islands, and to perform convergence studies in various numerical resolution parameters in both VMEC and PIES. The results shown here used 63 radial surfaces, 12 poloidal and 6 toroidal modes for the PIES calculation, and 49 radial surfaces, 9 poloidal and 5 toroidal modes for the VMEC calculation.

The application of SVD in this case identifies which coil harmonics are most pertinent to island formation. In this application we choose sufficiently many coil geometry harmonics to ensure there are more degrees of freedom than constraints, and the extra freedom is used to determine a solution with the minimal change to the coils. The coil harmonics varied correspond to the toroidal variation of the modular coils on a toroidal ‘winding-surface’. The winding-surface itself is not altered in this application, though this is possible as it is also described by a Fourier representation. The maximum coil alteration is about 2cm,

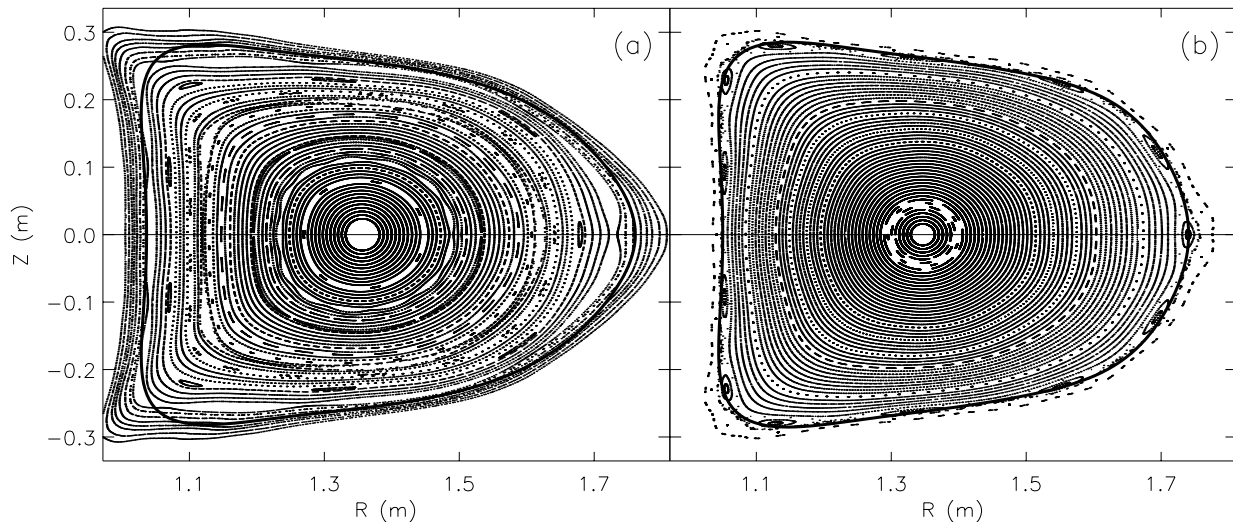


FIG. 4: Poincaré plots of equilibria with the healed coils: (a) the operating reference configuration using a multi-filament description, and (b) a vacuum case. The boundary of the corresponding VMEC equilibrium is shown as the solid line for each case.

which comfortably exceeds manufacturing tolerances, but is not so large that coil-healing significantly impacts other design concerns, such as diagnostic access. The healed coils are compared to the original coils in Fig.(3). On the scale of this figure it is difficult to notice the difference between the coils. That such a small coil change can produce a significant change in the quality of the equilibrium is reasonable considering that it is the resonant harmonics of the coil geometry that have been altered. Very small resonant error fields can give rise to significant islands, particularly where the shear is small.

#### 4. Flux surface quality of equilibria supported by healed coils and trim coil healing

The coil healing has assumed a filamentary model of the coils. The flux surface quality of the equilibrium supported by a finite cross-section of the coils was performed. A multi-filament coil set was generated to model the finite thickness of the healed coil set by replacing each filament of the original coil set with an array of 32 parallel filaments. The total envelope of the coil cross-section is 12 cm high by 10 cm wide. Without further healing, the flux surface quality of equilibrium consistent with the multi-filament coils as calculated by PIES remains intact, as shown in Fig.(4a). In fact, the surface quality appears to have improved, particularly near the edge.

With the geometry fixed, there remains freedom in variation of the coil currents and this freedom can be used to generate a variety of configurations to illustrate the flexibility of NCSX [17]. Various vacuum states were generated that preserve good-flux-surfaces, and one such state is shown in Fig.(4b).

To judge whether there are plausible and reasonable paths from vacuum fields to the desired NCSX target equilibrium, a discharge scenario was constructed. The discharge scenario is essentially a sequence of equilibria, with increasing  $\beta$ , that evolves the current profile in time self-consistently from the discharge initiation to the high  $\beta$  state. The evolution of the aspect ratio,  $a$ , plasma current,  $I$ , plasma  $\beta$ , and the rotational-transform on the axis and at the edge are shown in Table 1.

Table 1: Discharge Equilibria Sequence

| time (ms) | $a$   | $I$ (A) | $\beta$ (%) | axis $t$ | edge $t$ |
|-----------|-------|---------|-------------|----------|----------|
| 50        | 4.415 | 5.34e4  | 1.22        | 0.443    | 0.543    |
| 100       | 4.390 | 8.16e4  | 3.38        | 0.427    | 0.511    |
| 116       | 4.383 | 9.02e4  | 3.67        | 0.442    | 0.598    |
| 139       | 4.427 | 9.97e4  | 3.93        | 0.358    | 0.585    |
| 303       | 4.466 | 1.32e5  | 4.58        | 0.307    | 0.655    |

The width of magnetic islands depends in part on plasma pressure [9] and the pressure, current and rotational-transform profiles. As the configuration departed from the healed reference configuration, islands did re-appear as shown in Fig.(5); however, the island content of the healed coils was smaller than the island content of the original coils. An example of this is shown in Fig.(5d), which shows the Poincaré

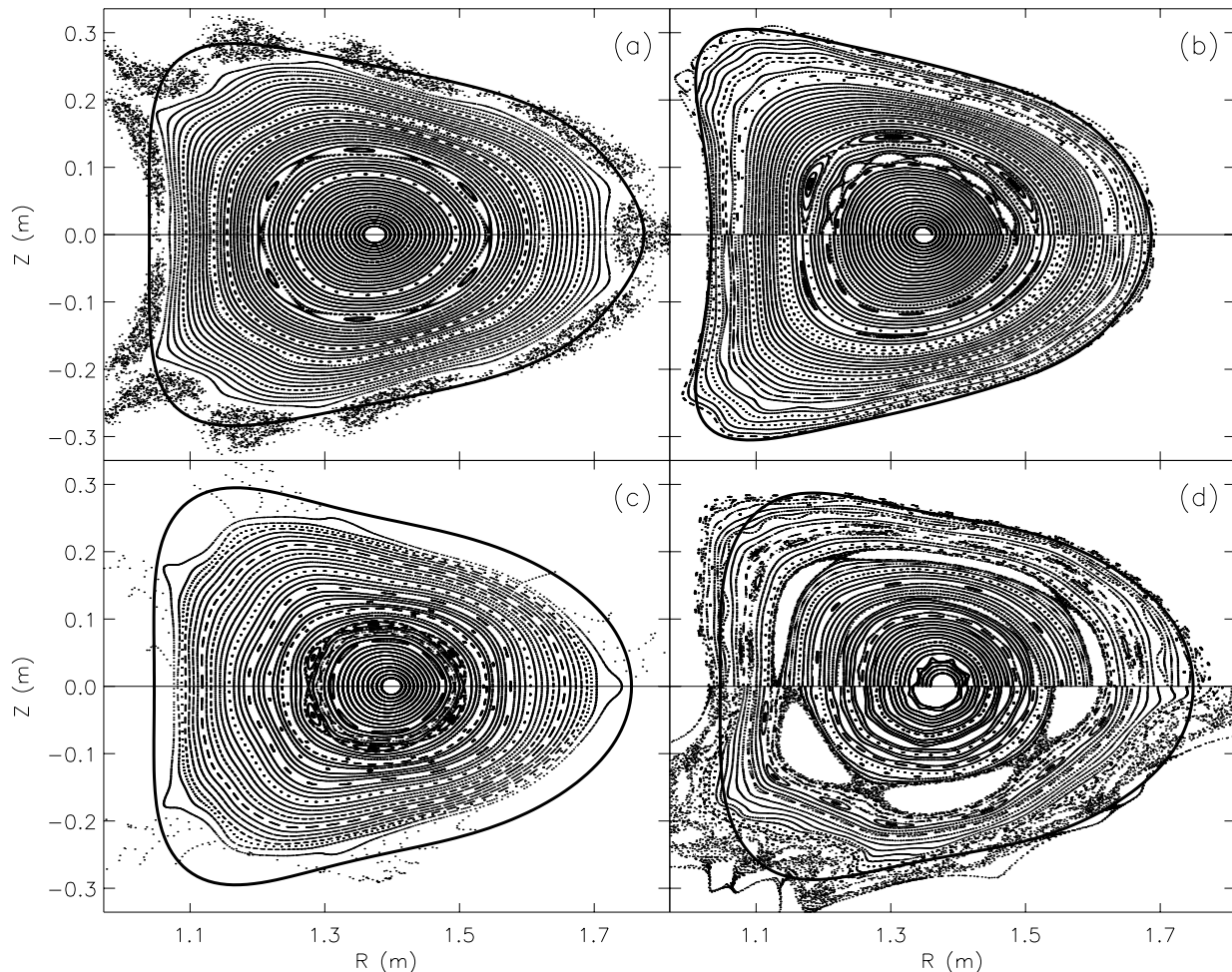


FIG. 5: Poincaré plots of the discharge configuration sequence: (a)  $t=50\text{ms}$  (b)  $t=100\text{ms}$  (c)  $t=139\text{ms}$  (d)  $t=303\text{ms}$  for the healed coils. In the lower half of (b), trim coils have been used to eliminate the  $(n, m) = (3, 6)$  island. In the lower half of (d), the original coils are used. The boundary of the corresponding VMEC equilibrium is shown as the solid line for each case.

plots for the 303ms equilibrium supported by the healed coils and the ‘same’ equilibrium supported by the original coils. The island content is smaller with the healed coils, and there are less chaotic field lines near the plasma boundary. Note that none of the discharge sequence equilibria were optimized with respect to surface quality and the current and pressure profiles are different to the profiles of the reference configuration.

To provide additional control of island widths as the configuration varies, the NCSX design includes arrays of  $m = 5$  and  $m = 6$  trim coils which provide control of the  $(n, m) = (3, 5)$  and  $(3, 6)$  resonances respectively. To determine the current required in the  $m = 6$  trim coil to suppress the  $(n, m) = (3, 6)$  island in the 100ms equilibrium, the method as presented in Section 2 was applied. In this case, the set of independent variables were chosen to be the trim coil currents, and the geometry of the modular coils was not changed. A trim coil current of about  $1\text{kA}$  was required, and the improvement in the flux surface quality is shown in Fig.(5b).

## 5. Comments

Present and future work on this topic includes the following: (a) Ballooning stability will be directly included as a constraint. In the results shown here, it was fortunate rather than design that ballooning stability was not substantially violated. It is preferable to *ensure* the healed plasma-coil configuration is ballooning stable. (b) The finite difference calculation of the coupling matrix  $\nabla B_{C_{ij}}$  involves  $M$  independent trial coil set evaluations. This aspect of the algorithm can be parallelized to achieve a great increase in speed. (c) The evaluation of the kink and ballooning stability is based on the free-boundary VMEC equilibrium for a given trial coil set. As there is potentially some slight discrepancy

between the VMEC and PIES equilibrium, a more consistent analysis will calculate the stability of the PIES equilibrium directly. (d) Additional constraints, such as specifying the location of the magnetic axis and the rotational-transform profile, may be included. With the particular application of this method to NCSX, for which great effort has been made to ensure the plasma is quasi-axisymmetric, the preservation of quasi-axisymmetry should be explicitly guaranteed. (e) It may be possible to design coils to simultaneously heal multiple configurations — to ensure an island free discharge evolution or to provide additional flexibility.

Presented is a stellarator design optimization routine that results in kink-stable plasma configurations with negligible island content and matching build-able coil-designs. In principle, by selecting additional high order islands, and allowing more coil parameters to vary, this method can reduce the islands to any desired level. In addition to the improvement in particle confinement, the construction of equilibria with good-flux-surfaces has implications for stellarator MHD stability calculations, which are usually based on equilibria artificially constrained to have nested flux surfaces. As the equilibria constructed using this method relax the unphysical imposition of nested surfaces, but maintain integrability by design, stability studies based on these equilibria are expected to be more reliable. The construction of integrable configurations provides the basis for comparison with codes that impose nested flux surfaces such as VMEC, and allows numerical investigation of the effect of perturbations on an integrable field. It will be interesting to determine how the equilibrium, in particular the island widths and associated chaos, behaves as a perturbation is applied and to compare with theoretical predictions [18].

We thank the NCSX design team, Raul Sanchez and Tony Cooper for use of the COBRA and TERPSI-CHORE codes. This work was supported in part by US Department of Energy contract DE - AC0276CH03073.

- 
- [1] D.K. Arrowsmith and C.M. Place. *An introduction to Dynamical Systems*. Cambridge University Press, Cambridge, U.K., 1991.
  - [2] S.R. Hudson, D.A. Monticello, and A.H. Reiman. *Physics of Plasmas*, 8(7):3377, 2001.
  - [3] M. Drevlak. *Fusion Technology*, 33:106, 1997.
  - [4] P. Merkel. *Nuclear Fusion*, 27(5):867, 1987;
  - [5] A.H. Reiman and H.S. Greenside. *Computer Physics Communications*, 43:157, 1986.
  - [6] A. Reiman, L. Ku *et al.* *Physics of Plasmas*, 8(5):2083, 2001.
  - [7] A.H. Reiman and A.H. Boozer. *Physics of Fluids* 27:2446, 1984.
  - [8] T. Hayashi, T. Sato *et al.* *Physics of Plasmas*, 1(10):3262, 1994.
  - [9] A. Bhattacharjee, T. Hayashi *et al.* *Physics of Plasmas*, 2(3):883, 1995.
  - [10] S.P. Hirshman, W.I. van Rij and P. Merkel. *Computer Physics Communications*, 43:143, 1986.
  - [11] S.P. Hirshman and O. Betancourt. *Journal of Computational Physics*, 96:99, 1991.
  - [12] D.J. Strickler, L.A. Berry, and S.P. Hirshman. *Fusion Science and Technology*, 41(2):107, 2002.
  - [13] R.L. Dewar, S.R. Hudson, and P. Price. *Physics Letters A*, 194:49, 1994.
  - [14] S.R. Hudson and R.L. Dewar. *Physics of Plasmas*, 6(5):1532, 1999.
  - [15] W.H. Press, B.P. Flannery *et al.* *Numerical Recipes in Fortran 77 : The art of scientific computing*. Cambridge University Press, Cambridge, U.K., 2nd edition, 1992.
  - [16] D.V. Anderson, W.A. Cooper *et al.* *International Journal of Supercomputer Applications and High Performance Computing*, 4:34, 1990.
  - [17] N.Pomphrey, R.Hatcher *et al.* *29th European Physical Society Conference on Plasma Physics and Controlled Fusion 17-21 June 2002, Montreux, Switzerland*.
  - [18] C.C. Hegna. *UW-CPTC*, 99-6, 1999.